Radboud University

Department of high energy physics

Bachelor thesis

The search for dark matter with AMS-02 antiprotons

Author:
Jochem Kip

Supervisors:
Prof. Dr. Wim Beenakker
Dr. Sascha Caron

July 4, 2017

Acknowledgments

I would like to thank my supervisors for helping me during this project and providing me with the opportunity to do research on this intriguing subject. I would also like to thank Melissa and Luc for helping me on various occasions when I got stuck again. For proofreading my thesis and correcting my linguistic errors my gratitude goes to Roland Hols. Lastly my thanks to Carmelo Evoli for guiding me through the process of understanding DRAGON.

Contents

1 Introduction

Since the dawn of man we have wondered what our universe looks like. From the grand structures of the cosmos to the most fundamental building blocks which make up our world. As our understanding of the universe gets better we realize there are some missing links. In the twentieth century it became clear that the galactic rotation curves did not match the expected values at the outer edges of the galaxy [1]. This was an indication of new physics and as the years progressed it indeed was. Since, as of this moment there is no consensus within the physics community as to why the galaxies rotate as they do.

One solution to this problem is to introduce extra mass distributed across the galaxy, which would explain the observed motion. This mass can be modelled as dark matter (DM), a massive particle which only interacts through gravity and the weak force, thus making it very hard to observe directly. The reason that this particle cannot interact through electromagnetism or the strong nuclear force is due to the fact that as of yet we have not seen it in accelerator experiments. If the particle has an electromagnetic interaction it would couple directly to photons and it would then be possible to observe a signal with one of the many telescopes used for astronomy. The reason that DM cannot have a strong nuclear interaction is because, if it would, some nuclei would have a higher mass than expected on the basis of its protons and neutrons because a DM particle would be captured in its nucleus. Both of these phenomena have not been seen and so it gives constraints on the properties of a DM particle. The standard model has no particles which can satisfy these imposed constraints so a new particle is needed, which is usually called a weakly interacting massive particle or WIMP for short.

There are some astrophysical observations that can determine the amount of dark matter in the universe. The before mentioned galactic rotation curves can be used to determine the DM distribution around said galaxy [2]. Another way is to measure gravitational lensing [3]. From general relativity we know that matter bends spacetime and so light passing through warped spacetime will seem to be bent to an observer assuming flat spacetime. Measuring the total deflection of the light can be used to determine the required mass to do so. With this data it can be determined that dark matter constitutes roughly eighty percent of the matter in our universe and twenty percent of the total mass density if we include dark energy [4].

At the moment there are numerous experiments trying to find conclusive evidence for dark matter but as of yet no definitive signal has been found. These experiments can be divided in three main categories of dark-matter produced signals: production, scattering and annihilation. With production the goal is to produce a DM particle. The production of a DM particle is often associated with standard model particles, most of which can be detected by a particle detector, and some energy which would appear to be missing. This energy is carried by neutrinos, dark matter particles or both, since these particles have a low chance of interaction with the detector they will not be detected and so their energy will appear to be missing when adding the energies of all the detected particles. These kind of searches are for example being performed at the LHC [5]. Scattering experiments try to detect DM when such a particle collides with ordinary matter. One of these experiments is LUX which uses liquid Xenon as a scattering target. When a DM particle collides with a xenon atom it gives off a light signal that can be detected [6]. The most relevant signal in our case however is that of annihilating dark matter. With this method one looks at the products of a DM particle colliding with another DM particle. This yields a distinct model dependent spectrum of various particles such as gamma rays, positrons and electrons, and antiprotons and protons. From their point of creation the charged particles will propagate through the galaxy as cosmic rays

(CR), to be detected at earth. There are however multiple sources of and uncertainties on the propagation of cosmic rays [7]. In combination with the simplifications of the chosen propagation model this makes finding a definitive signal difficult.
In this work the focus will be on the propagation of antiprotons and protons, as well as their respective ratio. As stated above both of these particles are produced when there is DM annihilation and for a given model the exact spectrum can be determined. With this information a possible dark matter signal could be detected with the antiproton over proton ratio. The reason this ratio is used instead of the other main candidate, which is the positron-electron ratio, is because there is less uncertainty on the production of antiprotons when compared to the production of positrons [10]. This is due to the available production channels, which are mainly nuclear collisions for antiprotons, while positrons can be produced by a variety of processes. This difference has to do with the fact that antiprotons are composite particles ($\bar{u}\bar{u}\bar{d}$) while positrons are elementary.

2 Theory

2.1 Dark Matter

In this work a supersymmetric model is used, more precisely the Minimal Supersymmetric Standard Model or MSSM for short. This entails that each particle in the standard model has a supersymmetric partner that has a larger mass and differs by spin 1/2, i.e. fermions are paired with bosons and vice versa [11]. One prediction is that all supersymmetric partners are unstable and will decay in known standard model particles except for one, the so-called neutralino. Since this particle is stable, massive and weakly interacting it fulfills the requirements of a WIMP and therefore dark matter.

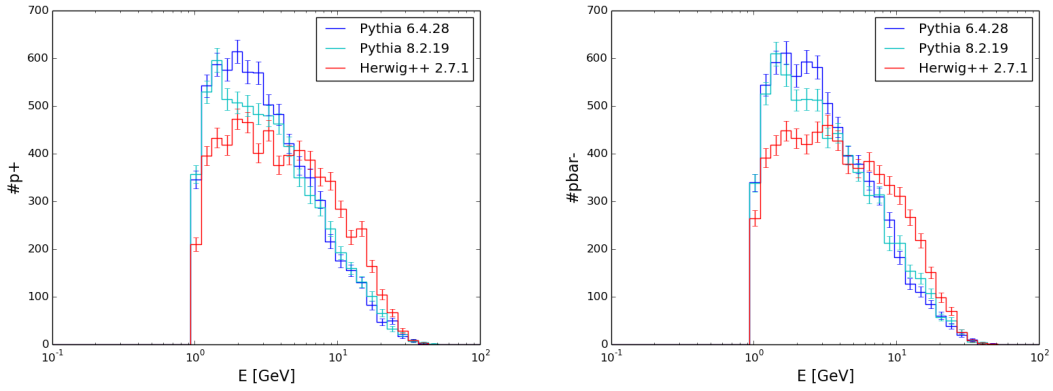

Figure 1: The absolute counts for both the antiproton and proton spectra with different simulation techniques for 10000 events. Source: J. Würzinger, *A Dark Matter Simulation of the Galactic Centre Photon Excess in the pMSSM and an Estimation of the Uncertainties, BSc. thesis (Radboud university, 2016)*

In this work a specific MSSM model is used that emerged from studies into gamma ray signals from

DM annihilation [8], [9]. The model uses the $\tilde{\chi}\tilde{\chi} \rightarrow W^+W^-$ annihilation path where $\tilde{\chi}$ represents the neutralino and W^+ and W^- are the W gauge bosons. Some of the interaction channels for the W^+ and W^- bosons result in the production of protons and antiprotons. Depending on the model utilised, a certain percentage of dark matter annihilations will result in the production of protons and antiprotons. Because the neutralino is a majorana particle (its own antiparticle) [12] a matter-antimatter production symmetry is expected. A quick glance at the annihilation channel will confirm this since the W^+ and W^- are each others antiparticle. With the use of monte carlo techniques the antiproton and proton spectra can be calculated. This has been done in a previous work [13] with three different programs, Herwig++ 2.7.1, pythia 6 and pythia 8. For our purposes we will use the data as made by pythia 8. From figure 1 we can see that the antiproton and proton production are roughly the same, which is to be expected due to the above mentioned symmetry considerations. It is worth noting that, although both Pythia 6 and 8 produce roughly the same spectrum, the one made by Herwig differs somewhat due to up to now unknown reasons. However, due to time constraints it is not possible to use all spectra, so only one was used, namely the spectrum produced by pythia 8.

2.2 AMS-02

The alpha magnetic spectrometer, or AMS-02 for short, is a charged particle detector in space, more specifically on the ISS. Being the most advanced charged cosmic ray detector to date the AMS-02 has produced the most precise CR measurements ever [14]. Having the ability to detect and identify multiple species of charged cosmic rays the AMS-02 yields new information on the propagation, composition and spectrum of cosmic rays.

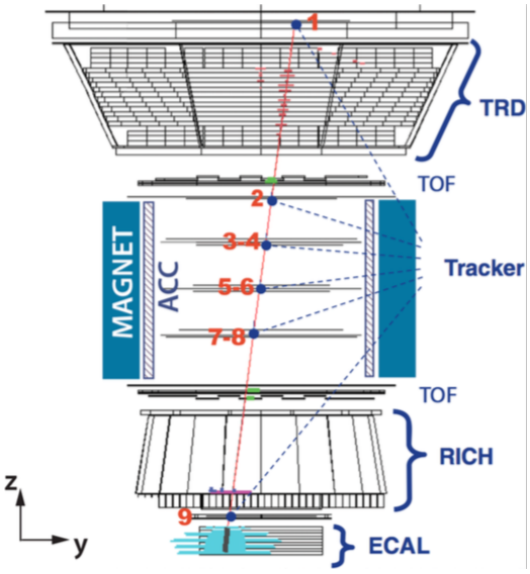

Figure 2: An example of an electron passing through the detector. Source: `https://inspirehep.net/record/1327686/files/fig01_detector.png`

The detector consists of multiple parts all working together measuring roughly 1000 events per second producing 1 Gbit/s of raw data. It composes of a transition radiation detector (TRD), four time of flight counters (TOF), a permanent neodymium alloy ($Nd_2Fe_{14}B$) magnet, nine silicon tracker planes (Tracker), multiple anticoincidence counters (ACC), a ring imaging Cherenkov detector (RICH) and an electromagnetic calorimeter (ECAL) [15]. After passing through the first silicone tracker the particles travel through the transition radiation detector to differentiate between $e^{\pm}$ and (anti)protons and identify heavier nuclei. After that the particles encounter the first time of flight counter giving the first data point for the velocity measurement and verification that the particle is moving downwards through the detector. This makes sure that only the particles that pass through all the different parts in the correct order are used, so an accurate measurement can be made. Next the particle encounters seven of the nine silicon trackers inside a magnetic field. The magnetic field gives a curved orbit to a charged particle, which can be tracked by the silicon planes providing information on the charge over mass ratio of the subject. On the sides of this tracker are anticoincidence counters. Since cosmic rays can come from all sides this instrument makes sure that no particles enter the detector through the side. After passing through the second time of flight counter the next encounter is the ring imaging Cherenkov detector, which independently measures the charge and velocity of the particle. Finally it passes through the electromagnetic calorimeter which measures the particle species and its shower energy and momentum.
The capabilities of AMS-02 go to the TeV scale, which in combination with its three independent classifications (TRD, RICH and ECAL) provide a detailed description of the cosmic ray spectrum [16]. Since these spectra had significantly larger uncertainties before AMS-02, either new physics can be discovered or more stringent constraints can be put on existing models.

2.3 CR propagation

2.3.1 The propagation equation

The journey of a particle through the Milky way is a true odyssey, a voyage fraught with diversions and reroutes. From its source to its destination, in our case the AMS-02 detector, the particle's path is determined by all sorts of influences. From local or galactic magnetic fields to interstellar gas [17]. The composition of cosmic rays is roughly 90% protons, 9% alpha particles and 1% consisting of other species like heavier nuclei, positrons and antiprotons [18]. Most cosmic rays come from stars at the end of their life cycle with the majority of cosmic rays coming from supernovae and pulsars [19]. After being injected into the interstellar medium the particles undergo all kinds of processes like diffusion, convection, collisions with interstellar gas etc. Since the Milky way is very complex and the uncertainties on variables like magnetic fields and interstellar gas are quite large, all models have to take this into account. The propagation of a particle through the galaxy can be modelled with the appropriately named propagation equation.
The propagation equation can take various shapes but the one used in this work is the following:

$$\begin{aligned} \frac{\partial N^i(r,z,p)}{\partial t} &= Q(r,z,p) + \nabla \cdot \left[(D_\perp \nabla - v_c) N^i\right] - \frac{\partial}{\partial p}\left[\dot{p} N^i - \frac{p}{3}\nabla \cdot v_c N^i\right] \\ &+ \frac{\partial}{\partial p}\left[p^2 D_{pp} \frac{\partial}{\partial p}\frac{N^i}{p^2}\right] - \frac{N^i}{\tau_f} - \frac{N^i}{\tau_r} \end{aligned} \tag{1}$$

This equation is written in cylindrical coordinates to make solving the equation as simple as possible, since the Milky way is assumed to be cylindricly symmetric. The left hand side of equation (1)

describes the time evolution of a certain CR species indicated by the density per total momentum of the CR species i: $N^i(r, z, p)$, with r the radial coordinate, z the height coordinate, both with respect to the Galactic centre, and p the momentum. The first term on the right hand side ($Q(r, z, p)$) is the source term, which can be split into two separate terms, one describing the ordinary injection, i.e. supernovae, pulsars, etc and one for dark matter. The ordinary injection term is too complex and the uncertainties are quite large so it is usually modelled as a broken power law, with its exact form depending on the propagation code utilized. The relevant information on this injection term is described in section 3.2.
The dark matter term for annihilating dark matter however is relatively simple. The chance per second for one dark matter particle to collide with another is $P = \langle\sigma v\rangle n$, the dark matter number density n times the averaged annihilation cross section weighted by the absolute value of the relative velocity of the annihilating DM particles $\langle\sigma v\rangle$. There are however multiple particles so the total number of collisions per unit volume per second becomes $\Gamma = \frac{1}{2}\sum_n \langle\sigma v\rangle n$. Here $\sum_n$ is the summation over the DM particles per unit volume and the factor $\frac{1}{2}$ is required to not count collisions twice, since particle N colliding with particle M is the same as particle M colliding with particle N. To get the total amount of antiprotons this expression has to be multiplied with the spectrum $\frac{dN_{\bar{p}}}{dE}$ per DM annihilation and the dark matter number density can be written as $\frac{\rho(r)}{m_{DM}}$ with $\rho(r)$ being the dark matter mass density profile and m_{DM} the dark matter mass. All of this combined becomes:

$$Q_{DM}(r) = \frac{1}{2}\sum_n \langle\sigma v\rangle n \frac{dN_{\bar{p}}}{dE} = \frac{1}{2}\langle\sigma v\rangle \left(\frac{\rho(r)}{m_{DM}}\right)^2 \frac{dN_{\bar{p}}}{dE} \quad (2)$$

The second part of the equation $\nabla\cdot(D_\perp\nabla - v_c)N^i$ represents the diffusion and convection. Diffusion is modelled with a diffusion coefficient that can take different forms for different assumptions. In this work it has been chosen as $D_\perp = D_0\beta^\eta g(r, z)\left(\frac{R}{R_0}\right)^\delta$. There are multiple important factors in this expression and since diffusion is an important factor in propagation they will be explained in detail. D_0 is a scalar that determines the strength of the diffusion and $\beta^\eta = \left(\frac{v_i}{c}\right)^\eta$ is a low energy correction factor, with v_i the speed of the particle being propagated. On first glance it would make sense that $\eta = 1$, however because this is a simplified model that does not encapsulate all processes it has been found that this factor can be tuned to model low energy processes like small perturbations in the galactic magnetic field [20]. From a physics point of view the next term is most interesting because this gives a spatial dependence to the diffusion coefficient, something usually modelled as spatially constant in most propagation codes. It has the following form: $g(r, z) = G(r)exp(\frac{|z|}{Z_t})$. As can be seen there are two coordinates since cylindrical symmetry is assumed. The radial part is still in a general form and in this work it is set at $G(r) = 1$. The height dependence is modelled as a simple symmetric exponential function normalized with the Z_t parameter to scale inversely proportional with the magnetic fields in the galaxy [20]. When looking at the Milky way it can be seen why this has been done. The reason why the height is taken to be absolute can be deduced from galactic symmetry, i.e. the top and bottom side are at least on a galactic scale the same and the Z_t factor determines the scale on which this expression increases. Lastly the rigidity dependence $\left(\frac{R}{R_0}\right)^\delta$, which has the largest impact on the propagation. With rigidity being defined as $R = \frac{pc}{Ze}$ or the momentum divided by charge, it influences the energy dependent spectrum. It also has a relatively simple form as a power law with exponent δ and normalized at R_0.
Since the first term is for diffusion it follows that the second ($\nabla \cdot v_c N^i$) term represents convection

by galactic winds with velocity v_c. The v_c term can be chosen so that it either has no spatial dependence or that it increases linearly as function of the height z. In this work it has been set to be constant.
Throughout its journey particles will gain and lose momentum by different processes, this can be seen in the third major term namely $\frac{\partial}{\partial p}\left[\dot{p}N^i - \frac{p}{3}\nabla \cdot v_c N^i\right]$. This term again has two distinct features with the first being the momentum loss or gain rate as $\dot{p} = \frac{dp}{dt}$. The gains or losses occur while propagating, so therefore it is represented by the time derivative of momentum. The second term indicates adiabatic energy losses.
The $\frac{\partial}{\partial p}p^2 D_{pp}\frac{\partial}{\partial p}\frac{N^i}{p^2}$ part of the equation signifies reacceleration. This is done by transforming N^i in momentum space with a spectrum and strength as defined by [21]

$$D_{pp} = \frac{4}{3\delta(4-\delta^2)(4-\delta)}\frac{v_A^2 p^2}{D_\perp} \tag{3}$$

Here δ is the exponent that appears in the rigidity dependence of the spatial diffusion coefficient, v_A is the Alfven wave velocity, p the momentum and $D_\perp$ is the spatial diffusion coefficient. The Alven wave velocity sets the speed of waves in a plasma on which particles can scatter.
The final part of the equation is $N^i/\tau_{f,r}$, which indicate losses by fragmentation and radioactive decay respectively, with $\tau_{f,r}$ being the mean fragmentation or decay time.

2.3.2 Magnetic fields

One of the most important aspects for charged cosmic ray propagation is the Galactic magnetic field. If the Milky way would have no magnetic fields charged cosmic rays could propagate in a fairly straight line from creation at distance r to detection by a detector with surface area A. In that case the chance of detection would be $\frac{A}{4\pi r^2}$. Using this ratio would result in a flux that is several orders of magnitude too low. However when magnetic fields are introduced the situation changes. Because charged particles follow magnetic field lines the particles are guided towards the solar system. This effect is amplified due to the fact that the solar system is located in one of the Milky way's spiral arms that has a relatively large magnetic field when compared to its surroundings [22].

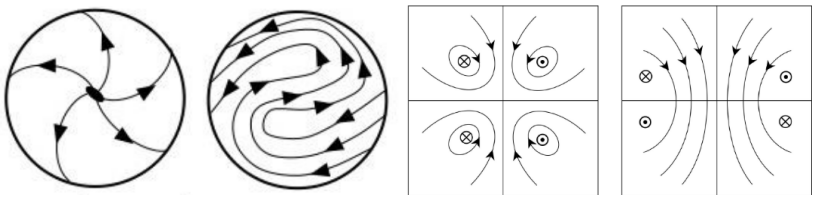

Figure 3: The disk field (left) with the axisymmetric (left) and bisymmetric (right) models. The halo fields (right) with symmetric (left) and anti-symmetric (right) configurations. Source: [24] and [25] for the disk fields and [23] for the halo fields

The average field strength in the interstellar medium ranges from roughly $0.1nT$ to $1nT$. For comparison the average magnetic field of the earth is $30\mu T$. The shape of the total magnetic field is still under discussion but there are useful details. The total magnetic field is usually divided in two parts, the field in the galactic disk and the field in the halo. Inside the disk the field is assumed to

have a form of rotational symmetry due to the shape of the Milky way. The two simplest models are an axisymmetric field where the field lines point outwards from the centre and curves anticlockwise and a bisymmetric field where the shape is like a heavily meandering river. Both models roughly follow the spiral arms and guide particles to or from the galactic centre.
The halo field also has multiple models where again the simplest two are the symmetric and anti-symmetric configurations. The symmetric situation has currents running parallel with respect to each other, this results in a shape where the field lines do not run through the galactic disk. The anti-symmetric case has currents running antiparallel, these field lines do run through the disk and form one large dynamo-like field, in contrast to the four separated fields in the symmetric case [23].
Since the velocity vector of a particle inside a magnetic field can always be decomposed into a part that points parallel to the field lines and a part perpendicular to it, every situation can be reduced to propagation following a magnetic field and circular motion with radius

$$r = \frac{\gamma mc\sqrt{1 - \left(\frac{mc^2}{E}\right)^2}}{qB} sin(\theta) \tag{4}$$

Plugging in the numbers it is found that the radius ranges from roughly 1 AU to 100 AU. This distance is fairly small on galactic scales but it does make it possible to escape more local fields. The synchrotron motion does decrease the energy of a particle via synchrotron radiation. This effect however is fairly small due to the high energy at which is propagated and the low energy of synchrotron radiation, namely radio waves.
There are also more turbulent magnetic fields, which are stronger and localized. They are mainly generated by local events like supernovae or star clusters [26]. When they are encountered during propagation the path can be vastly altered or the particle could be captured in the magnetic field. These phenomena can also affect particles at the start of propagation. Since many cosmic rays originate from events like supernovae these fields have an influence on the direction of propagation of the ejected particles.
One downside of magnetic fields is that the origin of cosmic rays are impossible to trace due to the constant deflection and uncertainties on the magnetic fields. This results in diffuse and point sources looking identical and the source location being completely unknown. This leads to a loss of information about the processes producing cosmic rays.
After the galactic journey the particles encounter the solar magnetic field. Through the so-called solar modulation, it has an effect on the lower energy part of the spectrum, i.e. below 5 GeV. The exact effect and strength of solar modulation varies from year to year depending on the current solar activity. The best way of determining the effect of solar modulation is to compare the results of different cosmic ray detection experiments from different times, since these record cosmic rays influenced by different solar modulation strengths. Another way is to look at the spectrum from Voyager-1 which is currently in the interstellar medium and therefore measures particles unencumbered by solar modulation [27], the downside being the age of Voyager 1 and with that the precision of its measurements.

2.3.3 Interstellar gas

Another important factor of propagation is interstellar gas, which can exist in three different forms: ionized, atomic or molecular. Ionized gas can be divided into two different categories, namely warm ionized and hot ionized. This difference is due to the process of ionization. In warm ionized gas a central star emits UV radiation which separates the electrons and its nucleus in the surrounding

gas, these stars are generally very massive. The ionization process of hot ionized gas is driven by the high temperatures of the gas itself. At the center of such clouds is usually a supernova or other event providing the required energy for ionization temperatures [28]. These types of gas are important in generating the large scale magnetic fields that dictate charged particle propagation paths.
The other two types are atomic and molecular gas clouds. The atomic clouds are mainly made up of hydrogen ($\sim 90\%$), helium ($\sim 9\%$) and a small fraction of heavier elements ($\sim 1\%$). These clouds are typically of very low density, meaning collisions rarely occur. Often located between stars the atoms receive but little energy and as a result reside mostly in their energetic ground state. Molecular gas consists mainly of H_2 and small traces of carbon based molecules like CH, CN or CO, although more complicated molecules are possible following random collisions.
The densities of clouds can vary from 10^{-4} to 10^6 atoms per cubic cm depending on which kind of material it is comprised of and where it is situated. Typically molecular and warm ionized gasses are the densest while atomic and hot ionized gasses are more sparse. The densest regions are located around stars or star remnants. When looking at less localized regions the spiral arms generally have the highest gas density [28].
There are several effects on propagation from the gas clouds. First of all these gasses form galactic winds transporting material from one place in the galaxy to another. When looking at the general composition of the interstellar material it can be seen that it is roughly the same as the composition of cosmic rays and this is no coincidence when looking at the movement of the solar system and the local interstellar medium. Because both are moving with respect to each other there will be material passing into the heliosphere and some of it will be detected at earth.
Secondly there are particles being created by collisions between cosmic rays and particles in the clouds. These collisions produce different kinds of nuclei like lithium, beryllium and boron and also antiprotons.

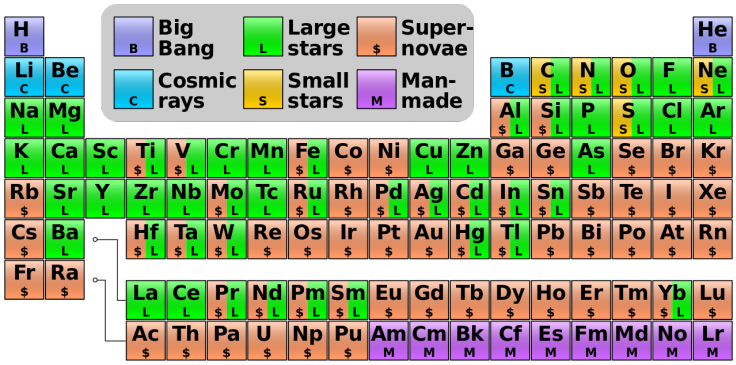

Figure 4: The main sources for all elements of the periodic table. Source:`https://upload.wikimedia.org/wikipedia/commons/thumb/3/31/Nucleosynthesis_periodic_table.svg/512px-Nucleosynthesis_periodic_table.svg.png`

The production of boron yields important information since it is only produced during cosmic ray propagation [29]. Carbon is mainly injected into the cosmic ray spectrum by exploding stars and the spectrum does not change much during propagation. So when the ratio of boron and carbon

is used this gives constraints on the parameters of propagation models of both the production and propagation of other species of cosmic rays, since it can be assumed that the circumstances are the same for all particles.
Antiprotons are also mainly created by nuclear collisions between cosmic rays or cosmic rays colliding with nuclei inside gas clouds. The products of these collisions are called secondary antiprotons. It is also possible for products of a previous collision to collide again and produce new antiprotons, these are called tertiary antiprotons. Secondary and tertiary antiprotons are indistinguishable when they are detected, they are however important for a model simulating propagation. The same reasoning applies for other particles like protons, so when protons are produced by collisions they are called secondary protons. Theoretically a particle could be produced by the n^{th} collision and would carry its respective name. The contribution of these processes is negligible at different values of n for different cosmic ray species. For example: tertiary antiprotons are still significant, while tertiary protons can be neglected.

3 Research

3.1 The AMS-02 data

Since the start of the AMS-02 experiment in 2011 it has measured a variety of cosmic ray species. In this work two spectra are used, namely the ratio of antiprotons over protons and the ratio of boron over carbon. The precision of both of these ratios has vastly improved over previous data, with the experiment before AMS-02 being PAMELA (Payload for Antimatter Matter Exploration and Light-nuclei Astrophysics). The improvements are largely in the higher energy range above roughly 10 GeV, as can be seen in figure 5.

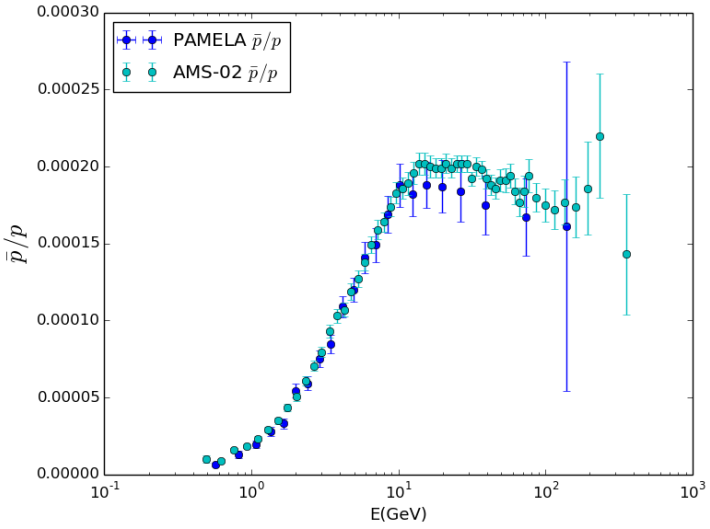

Figure 5: The AMS-02 ratio of antiprotons and protons in comparison to the PAMELA data

The total error on all points has been decreased and the spectrum at higher energies has shifted to the top of the PAMELA errorbars. Since PAMELA has larger errors and lies lower than AMS-02 from 10 GeV onwards, most models tuned with the PAMELA data were unable to explain the high-energy end of the spectrum. When looking at the general shape it can be seen that from 1 GeV the ratio rises until about 10 GeV after which the ratio starts to straighten or drop slightly. It should be noted that the plot is made with the x-axis plotted logarithmically and the y-axis linearly for display purposes. At 15 GeV there is a small set of points fluctuating up and down, this is most likely due to the relatively small amount of events and the systematic error on the measurement, which is of the same size as the fluctuations. Naturally at higher energies the number of events drops. To give an indication, at 2 GeV the antiproton flux is 1.40×10^{-2} [m^2 sr s GeV]$^{-1}$ while at 30 GeV the total flux is 2.68×10^{-4} [m^2 sr s GeV]$^{-1}$, both within a margin of error that is two orders of magnitude smaller.
The other relevant ratio is that of boron over carbon. Below the older PAMELA data and the most recent AMS-02 data can be seen.

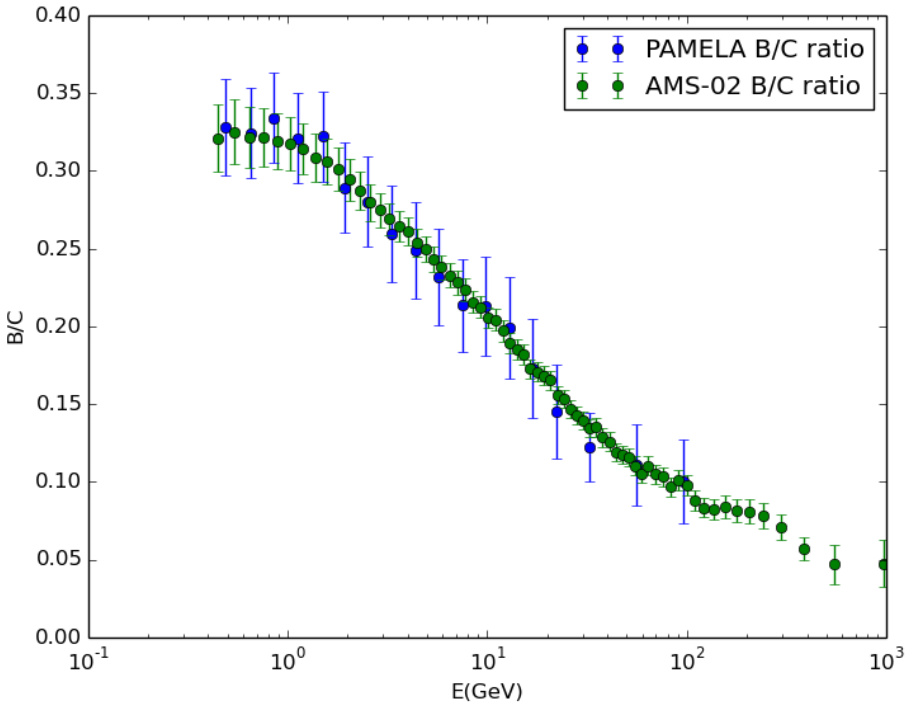

Figure 6: The PAMELA and AMS-02 boron-carbon ratio as a function of energy

The ratio has remained roughly the same although the AMS-02 ratio varies less when looking at the points, giving rise to a smoother line. But more important is that the error on the data has been reduced significantly allowing for stronger constraints. The AMS-02 data also indicates a small

increase in the ratio from 100-500 Gev, the exact reason for which is unknown. The uncertainties of the entire spectrum have been reduced providing strong constraints, except at energies around 1 GeV where a variety of shapes is allowed. The dropping of the ratio indicates either a higher injection flux of carbon at increasing energy or a dropping of higher energy boron production during propagation. The latter would imply that the production of cosmic rays during propagation declines at higher energies. However, this interpretation has to be handled with caution because while it is reasonable to assume that various variables are similar for all species, like magnetic fields, gas clouds, etc, the production cross section is not. Therefore the boron-carbon ratio is a useful tool for constraining cosmic ray propagation, but it has to be kept in mind that it does not include all variables for all species so small variations are possible.

3.2 DRAGON

The propagation equation is solved using DRAGON (Diffusion Reacceleration and Advection of Galactic cosmic rays: an Open New code) [30]. Consider the following one dimensional differential equation.

$$\frac{\partial N}{\partial t} = D\frac{\partial^2 N}{\partial x^2} \tag{5}$$

One way to solve this numerically is to use a Cranck-Nicholson scheme, which is the way DRAGON does it [31]. This method divides the time and spatial variables in discrete parts with width Δt and Δx, respectively, and solves the equation with the following algorithm:

$$\frac{N_i^{n+1} - N_i^n}{\Delta t} = \frac{D}{2}\left[\frac{(N_{i+1}^{n+1} - 2N_i^{n+1} + N_{i-1}^{n+1}) + (N_{i+1}^n - 2N_i^n + N_{i-1}^n)}{(\Delta x)^2}\right] \tag{6}$$

Here N indicates the differentiated function, n the position in the time grid and i the position in the spatial grid. This formula is only valid for the one dimensional case mentioned above, so the scheme has to be updated in order to be able to compute the entire propagation equation. To realise this the algorithm can be extended to accommodate the extra spatial and momentum dimensions. By using operator splitting this can be written in a number of separate steps. Consider the differential equation

$$\frac{\partial N}{\partial t} = \lambda N \tag{7}$$

where the operator λ can be written as a sum of operators λ_i, so $\lambda = \sum_{i=1}^{l} \lambda_i$. If for each λ_i a differencing scheme U_i can be calculated, then the time evolution from n to n+1 can be computed as

$$\begin{aligned} N^{n+1/l} &= U_1(N^n, \Delta t) \\ N^{n+2/l} &= U_2(N^n, \Delta t) \\ &\dots \\ N^{n+1} &= U_l(N^n, \Delta t) \end{aligned}$$

So each time step of Δt has to undergo l transformations to encompass all operators for every timestep. The exact form of all U_i is dependent on the operators and all terms can usually be rewritten in a more compact form. This method has been proven to be numerically stable [32] providing reliable solutions.

DRAGON uses an xml-file as input, so all variables have to be edited here (see the appendix for the complete file). The entire program is run in several different steps with the first being the creation of the spatial grid and energy array. The Milky way is modelled as a cylinder where both the radius and height are variables, so these have to be defined together with the number of grid points in both the radial and axial direction. It is possible to propagate both in 2D and 3D, where the difference is that the angular dimension is not used in 2D mode while it is in 3D. In this work the 2D mode is used because of time restraints, bearing in mind that one run in 3D mode is roughly a factor thirty longer when compared to a 2D run with otherwise similar input.
The energy array is filled using the following formula, $E_i = \exp(\ln(E_{min}) + i\ln(E_{factor}))$, with E_{min} being the lowest energy, here set at $E_{min} = 0.1\ GeV$, and $E_{factor} = 1.2$ being the step size with which the array grows over one iteration. The process will be be continued up to a maximum energy E_{max}, which is in this work defined as $E_{max} = 1000\ GeV$. All energies are kinetic and given in GeV. The output file gives the propagated species as GeV/nuc, which only matters for helium nuclei and heavier, since nuc=1 for electrons, positrons and (anti)protons.
The process for time iteration, which comes after the creation of the energy array, is a little different. Starting from a large Δt (Δt_{max}) one works to a small one (Δt_{min}) by applying a rescaling factor Δt_{factor} after a number of steps N_{rept}. Using the DRAGON default values one starts at 64 Myr and after 30 steps the scale is resized by a factor of 0.25 which is repeated until one reaches a value of 0.001 Myr. This means a total of 8 resizes are needed, which correspond to a total of 240 iterations. These timescales vary a lot to be able to reasonably calculate all physical processes occurring in the galaxy while keeping the computing time low.
Next all the variables are read that are needed to calculate the propagation. Starting with variables concerning supernova remnants, which gas model is used and what densities and compositions are implemented. The next set has to do with the shape of the diffusion coefficient, reacceleration and magnetic field strength and shape. The diffusion variables are the same as described in section 2.3.1. Here the radial part of the diffusion coefficient is set to be one due to the uncertainties on this factor and the reliability of the output. The reacceleration is determined by two variables, the Alfven wave velocity and which precise model is used. For the magnetic field the shape has to be chosen and the strength for the halo, disk and turbulent fields has to be set.
The normalization and injection procedure of DRAGON will now be discussed. Starting with the normalization a value has to be given for a specific energy for a few different species, electrons, protons and optionally antiprotons. Because in this work the focus lies on antiprotons the normalization of this species is used. Since there are many sources of cosmic rays it is impossible to model this accurately, so a broken power law is used. The DRAGON default has three breaks, which is also used in this work. The source term has the following general form.

$$Q_i(r, z, R) = Q_0 q_{SN}(r, z)\Phi(R)\exp\left(-\frac{R}{R_c}\right) \tag{8}$$

Where R is the rigidity, Q_0 is a normalization factor, $q_{SN}(r, z)$ provides a spatial dependence based on supernovae observations, $\Phi(R)$ is the injection spectrum, which in our case has three breaks, and R_c is the cut-off rigidity. The $\Phi(R)$ function defines the rigidity shape before propagation and is modelled as a broken power law with multiple breaks. The i'th break is given by R_{i-1}, so the first break is given by R_0, the second by R_1 etc. The breaks divide the rigidity spectrum in pieces, with the exponents for rigidities lower than a break R_i given by $-\alpha_i$ and for rigidities higher than R_i by $-\alpha_{i+1}$. For rigidities below a break R_i the function has the following form:

$$\Phi(R) = f_i R^{-\alpha_i} \tag{9}$$

With f_i being a smoothing function defined as follows:

$$f_i = \begin{cases} 1 & i = 0 \\ \Pi_{j=0}^{i-1} R_j^{\alpha_{j+1}-\alpha_j} & i \neq 0 \end{cases}$$

Lastly the variables for dark matter production have to be given. This starts with the way dark matter produces particles, which is either decay or annihilation, followed by the spectrum of the production and the dark matter profile. In this work annihilation is relevant with the spectrum mentioned in section 2.1. The chosen dark matter profile is NFW with a local density of 0.41 GeV/cm^3. The species propagated are leptons and antiprotons. There are no protons propagated because the command required is not known and it can be assumed that the propagation for antiprotons and protons is the same when averaged over large numbers. The main difference between antiprotons and protons regarding propagation is their charge, and therefore their interaction with magnetic fields. However, the effect of a magnetic field on a charged particle depends on the angle between the field lines and the velocity vector of a particle. When averaging over large numbers of particles and assuming uniformly distributed angles this results in a symmetry for charges with opposite signs. For the mass of the dark matter particle 85 GeV is used since this is the value used in the MSSM model that was utilised for calculating the spectrum. The velocity weighted cross section $\langle \sigma v \rangle$ is set to be a variable.

3.3 Search method

To find the best fit the following parameters are used: $L, D_0, \delta, \eta_T, v_A, Z_t, \alpha_0, \rho_0, \alpha_1, \rho_1, \alpha_2, \rho_2, \alpha_3$ with in addition $\langle \sigma v \rangle$ for a fit with dark matter. These parameters can be divided in four categories with the first defining the edges of the galaxy: the outer radius of the Galaxy is fixed at 12 kpc and L defines the halo height. The second set consists of $D_0, \delta, \eta_T, v_A, Z_t$, which defines the diffusion coefficients of both ordinary space and momentum space as described in section 2.3.1. The injection spectrum is entirely fixed by $\alpha_0, \rho_0, \alpha_1, \rho_1, \alpha_2, \rho_2, \alpha_3$ as set by the DRAGON injection spectrum. With α_i being the exponent in the broken power law and ρ_i the break in rigidity. The last variable is the velocity weighted cross section $\langle \sigma v \rangle$, which determines the amount of injected dark matter particles.
The quality of the fit is measured by calculating χ^2 which is defined as

$$\chi^2 = \sum_{i=0}^{N} \left(\frac{Data_i(E) - Model_i(E)}{Error_i(E)} \right)^2 \tag{10}$$

Here $Data_i(E)$ is the energy dependent spectrum of a cosmic ray species i as provided by AMS-02, $Model_i(E)$ is the spectrum provided by DRAGON for the same species i and $Error_i(E)$ is the uncertainty of the spectrum provided by AMS-02. For the fit of multiple data sets $\chi^2 = \chi^2_{set_1} + \chi^2_{set_2} + \dots$ is used. A better fit will result in a lower χ^2 since this number is low when model points lie close to the data points relative to the error from that data point. A positive value is always guaranteed since for each point the value is squared. A good χ^2 is when its value is close to or below the total degrees of freedom, i.e. the number of data points minus the number of parameters.
The fit has been done with the use of two different spectra, specifically the antiproton over proton ratio and the boron over carbon ratio. To find a possible dark matter signal, the background and

background with dark-matter produced particles both have to be fit. These two scenarios have been fitted with respect to only the antiproton over proton ratio and that ratio in combination with the boron-carbon ratio to constrain propagation parameters. The total number of parameters is 13 for the background, which becomes 14 for a background fit with dark matter due to the addition of $\langle \sigma v \rangle$. The bin size for $\bar{p}/p$ is 57 and for B/C it is 67, so the degrees of freedom are 44, 43, 111 and 110 for background and background with dark matter for $\bar{p}/p$ (first pair) and $\bar{p}/p$ with B/C (second pair).
To calculate χ^2 the data from the model has to be in the same bins as the AMS-02 data in order to be able to subtract it. To accomplish this the model is assumed to be smooth between points, so a spline can be used that goes through all points in such a way that a smooth line goes through all points. The resulting spline is then used to create an array with points in the correct bin either from $\bar{p}/p$ or B/C, so that χ^2 can be determined.
A particle filter was used to find the minimum. An array of the three best fits is created and a random number generator selects one of these. The parameters are then used as the center of a gaussian with a width depending on the value of the quality of the fit. The width has been set at 0.5 for χ^2 of 500 and up, 0.1 for a value between 500 and 100 and lastly 0.01 for 100 and lower. The gaussian, and the associated width, is scaled to the size of the scanned range for a parameter. For the combined fit of both $\bar{p}/p$ and B/C the lowest width of 0.01 starts at a χ^2 of 150 due to the increased degrees of freedom.
The correct way to use a particle filter is to randomly generate a set of points and then select a subset of best values. This subset is then used as the center of the previously mentioned gaussian with a fixed width, which is for the first cut usually 0.5. After generating another set of points a second cut is made with a better χ^2 and the process starts over. After each cut the gaussian can be set at some width, which for later iterations can be reduced to search more locally around a selected point. Since this method has not been used, for all interpretations of the data we have to keep in mind that the results are most likely in a local minimum. This is because the method utilised improves upon a single point until a minimum is reached, after that a width of 0.01 is not sufficient to reach other points in the parameter space. After points are generated as described above they are put into the xml-file that DRAGON uses as input. The xml-file that was used is given in the appendix with parameters indicated as 'variable'. Using this file as input DRAGON calculates the spectrum and writes it in a text file, which can be read by a python script that can calculate χ^2. That script imports the AMS-02 and DRAGON data and uses that for χ^2, after which it checks the value against the current best value. If the new value is better the parameters are written to a file for the best fits and the highest value is removed and also to a file where all points are stored regardless of its value.

4 Results

4.1 Impact of dark matter production

To see the effect of a potential dark matter signal it is important to know on which part of the spectrum it has an effect and if it is a significant contribution. To find the order of magnitude of the dark matter produced (anti)protons a DRAGON fit is used. This gives a good indication of possible production since any calculation by hand cannot take into account the magnetic fields, interstellar environment etc.

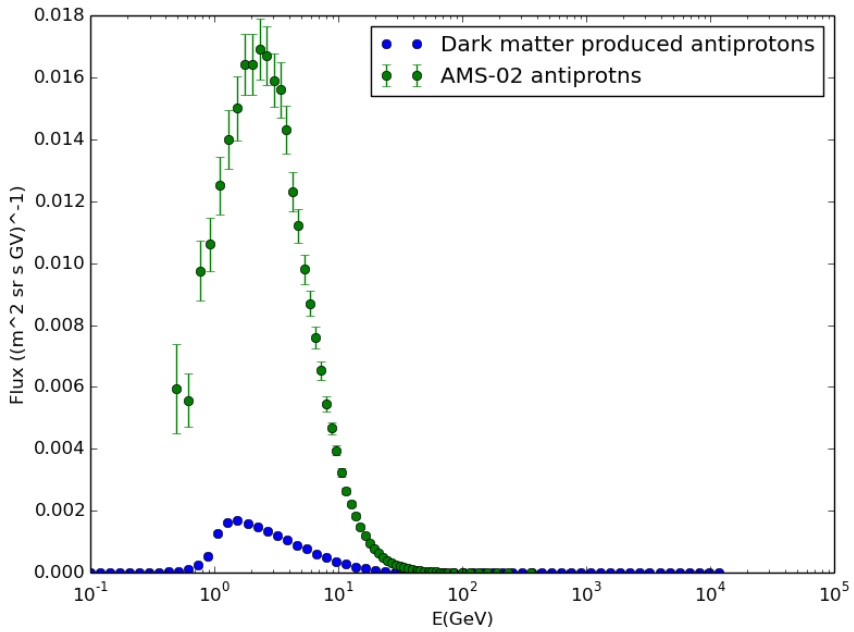

Figure 7: The antiproton flux produced by dark matter annihilation in comparison to the antiproton flux measured by AMS-02.

The antiprotons produced by dark matter annihilation is within or close to the order of magnitude of the antiproton flux as can be seen in figure 7. The spectrum of figure 1 is used and the shape can still be recognised although it has been smoothed as is expected during propagation. The increase at 1 GeV is due to the shape of the spectrum provided in section 2.1, which also has an increase at 1 GeV. The difference being that due to energy losses this spectrum has smoothed, resulting in antiprotons with an energy lower than 1 GeV. From 1 GeV onwards it follows roughly a decreasing shape until 25 GeV. While at 1 GeV the production is the highest it is the relative production that is important, since

$$\frac{\phi_{\bar{p}}}{\phi_p} = \frac{\phi_{sec_{\bar{p}}} + \phi_{tert_{\bar{p}}} + \phi_{DM_{\bar{p}}}}{\phi_{prim_p} + \phi_{sec_p} + \phi_{DM_p}} \tag{11}$$

To see where the production has the largest effect, figure 8 gives an indication.

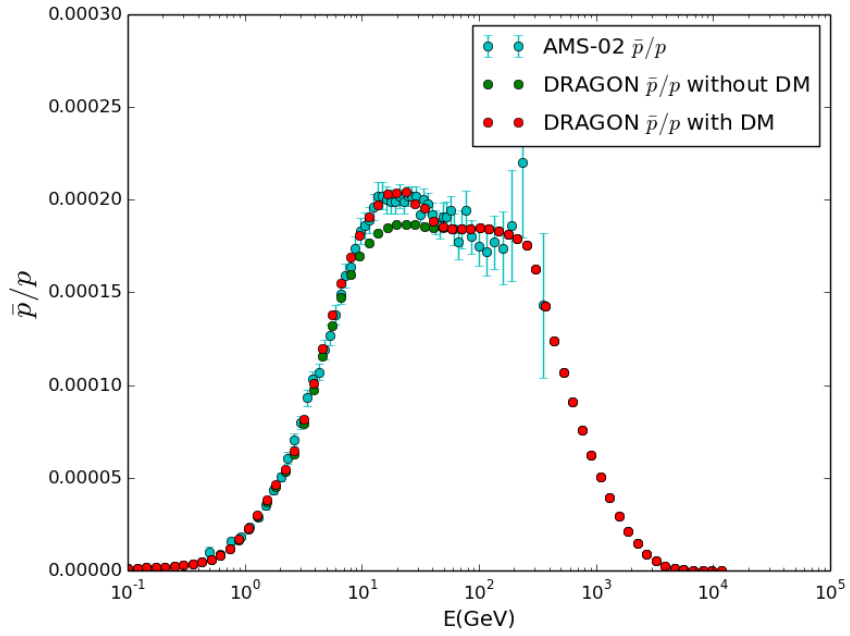

Figure 8: The difference between antiprotons and protons as produced by dark matter and background, compared to the background only scenario with the same parameters.

Figure 8 serves only as an indication of where dark matter annihilation affects the ratio, since the figure is produced from a fit of background with dark matter to the observed ratio, so a bias is introduced when the same parameters are applied to a background-only scenario. However, varying the parameters does not significantly alter the location of the effect since all parameters apply to all propagated particles with the exception of $\langle \sigma v \rangle$. So if the background spectrum increases or decreases at a certain energy the dark matter produced spectrum will do the same. A decreased value for $\langle \sigma v \rangle$ only affects the number of dark matter annihilations and therefore the amount of produced particles, resulting in a lower signal but not in a shift of the spectrum.

4.2 The fit without B/C

For the initial round of scans just the $\bar{p}/p$ ratio was fit for two scenarios, a background fit and a background with contribution from dark matter annihilation. For the calculation of χ^2 all the data points were used, which is 57 in total. The result for just the background can be seen in figure 9. As can be seen the model lies close to all the points below roughly 50 GeV, this is not surprising bearing in mind that the uncertainties of those points are low and the quality of the fit is determined with χ^2. From this energy onwards, however, the uncertainties become larger, giving the possibility for a variation in the slope. The fit has $\chi^2 = 31.9470073697$, which for 44 degrees of freedom yields a p-value of 0.911898.
The result for the background with an addition of dark matter produced particles can be seen

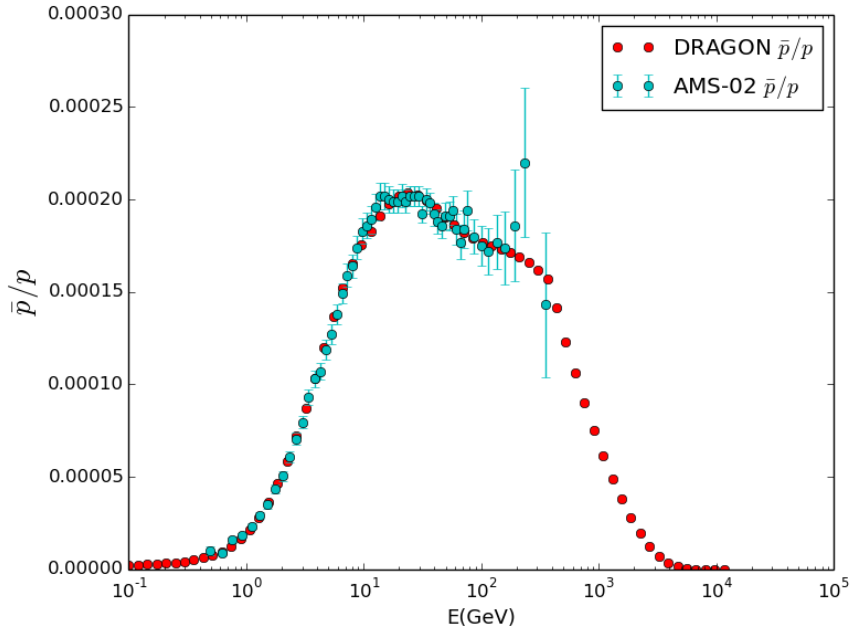

Figure 9: The $\bar{p}/p$ spectrum as measured by AMS-02 and modelled by DRAGON for the background only scenario.

in figure 10. As mentioned, the slope can differ from 50 GeV onwards, which is exactly the case when compared to the previous fit. This is most likely due to the addition of extra (anti)protons from dark matter. The background fit has to accurately model all the data with just the injection spectrum, allowing for less freedom. So when the ratio starts to drop at 20 GeV, the fit has to keep dropping, while the dark matter contribution is exactly at that energy giving the freedom to have a flat ratio.
With the addition of dark matter as a source the result is $\chi^2 = 39.7234488815$ for 43 degrees of freedom, corresponding to a p-value of 0.61422. There are however two remarks on these results. First of all it is likely that these fits are the local and not global minima due to the search method employed. Secondly there has been no check if the parameters are physically correct. This is usually done with the boron over carbon ratio. When plotting the B/C ratio as measured by AMS-02 and modelled by DRAGON with the parameters acquired with the fits of the $\bar{p}/p$ data it will give an indication if the parameters correspond to an accurate propagation scenario.
Figures 11 and 12 give the modelled B/C spectrum in comparison with the AMS-02 measurement for the background and background with dark matter, respectively. While the dark matter fit is significantly better than the background fit both do not provide a good fit. From the figures it can be seen that over the entire energy range the modelled ratio differs, while in the antiproton over proton ratio the dark matter contribution is fairly localized. This implies that it is not the actual protons or antiprotons coming from dark matter that has the largest effect on the model, but more so the effects of different requirements for the injection and propagation parameters.

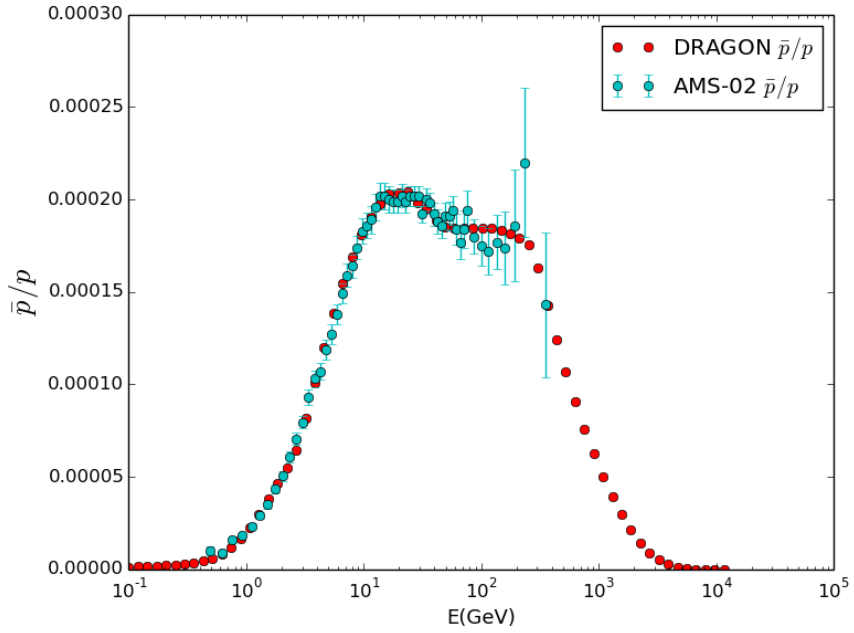

Figure 10: The $\bar{p}/p$ spectrum as measured by AMS-02 and modelled by DRAGON for the background with a dark matter contribution

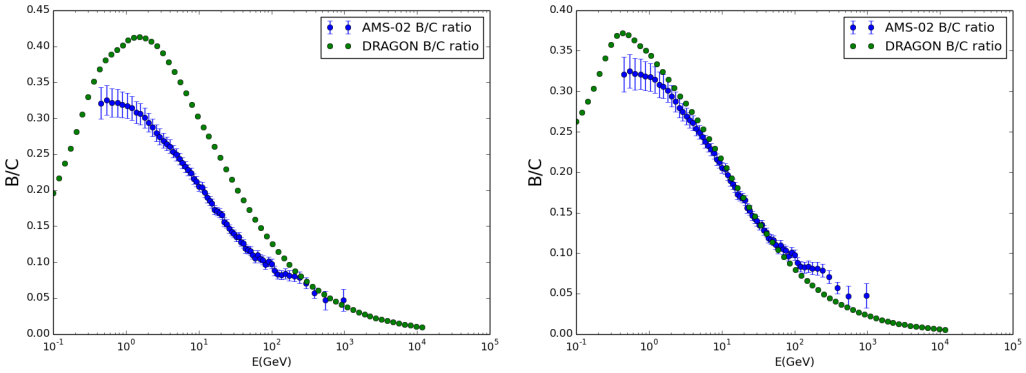

Figure 11: The B/C ratio as modelled by DRAGON with the parameters from the $\bar{p}/p$ background fit (left) and background with dark matter (right).

4.3 The fit with B/C

As seen in figure 11 the difference between the AMS-02 boron-carbon ratio and the output from DRAGON is substantial. Since this ratio is important for determining whether or not the propaga-

tion parameters are plausible, therefore a second round of scans is needed to fit both the $\bar{p}/p$ and B/C ratios to give a more accurate description of reality.

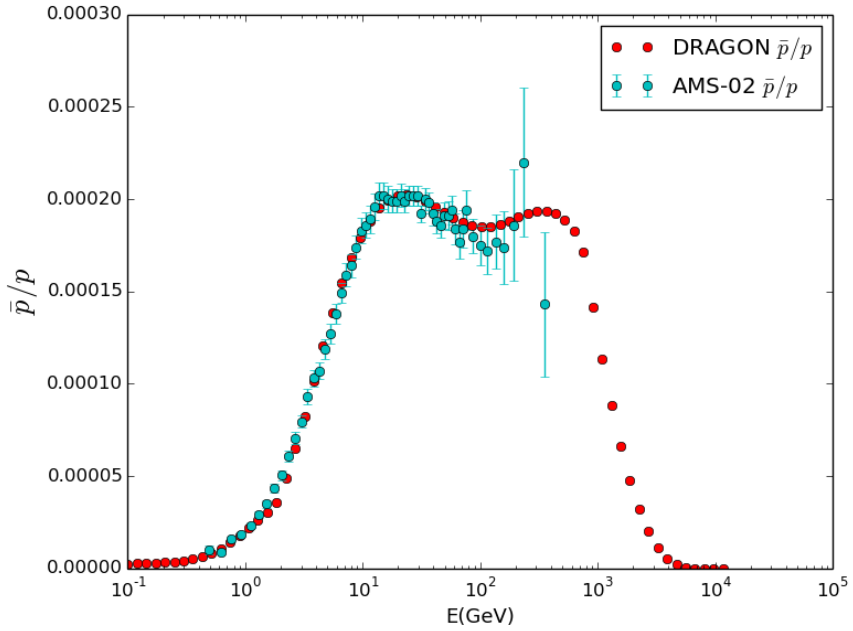

Figure 12: The background fit for the $\bar{p}/p$ data as measured by AMS-02 and modelled by DRAGON.

The fit for a background only scenario has $\chi^2 = 151.58810363$, which for 111 degrees of freedom corresponds to a p-value of 0.006354. From figure 12 it can be seen that this ratio fits fairly well and smooth with some exception from 100 GeV onwards when the model seems to go up slightly. From the boron-carbon ratio in figure 13 it becomes clear where the discrepancy is residing. Between 0.5 and 10 GeV the model underestimates the ratio, implying too much carbon injection, too little boron production or both. However, when looking at the antiproton over proton data a small underestimation can be observed, but not of such width or size. It should again be acknowledged though that this is most likely a local minimum, so these results have to be used with caution.
In figures 14 and 15 the fits are presented where an extra dark matter component is present. With $\chi^2 = 75.6660035271$, 110 degrees of freedom and a p-value of 0.99486 the fit is significantly better than the scenario without dark matter, but again this could be due to a local minimum in the background-only fit. With the exception of the slight bump at 300 GeV in the B/C ratio, the model can explain all data satisfactorily as is indicated by the value of χ^2. While the fit through $\bar{p}/p$ is not as horizontal as in figure 10, it is still fairly straight as is expected taking into account the location of the dark matter signal.

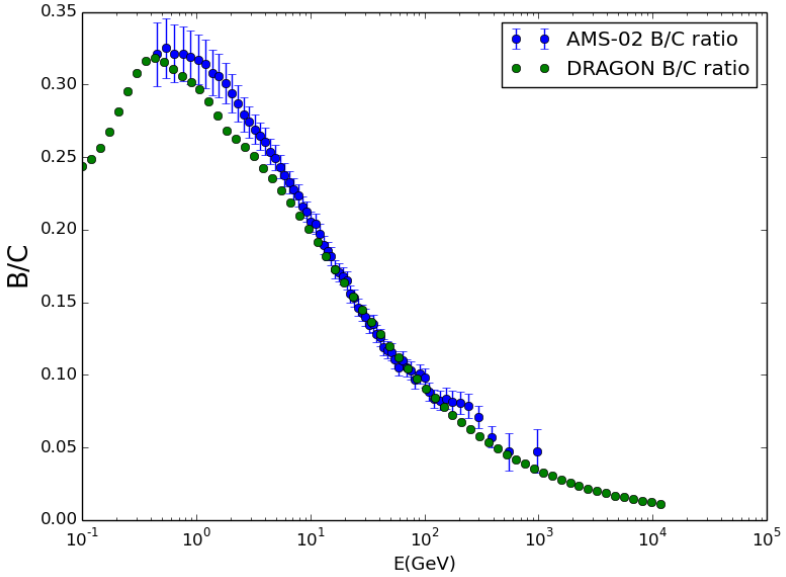

Figure 13: The boron-carbon ratio as measured by AMS-02 and modelled by DRAGON.

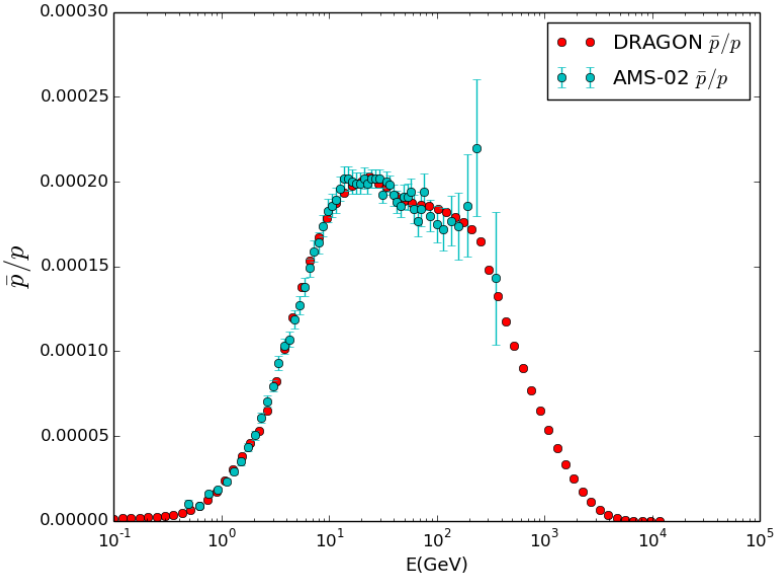

Figure 14: The $\bar{p}/p$ fit for background with dark matter

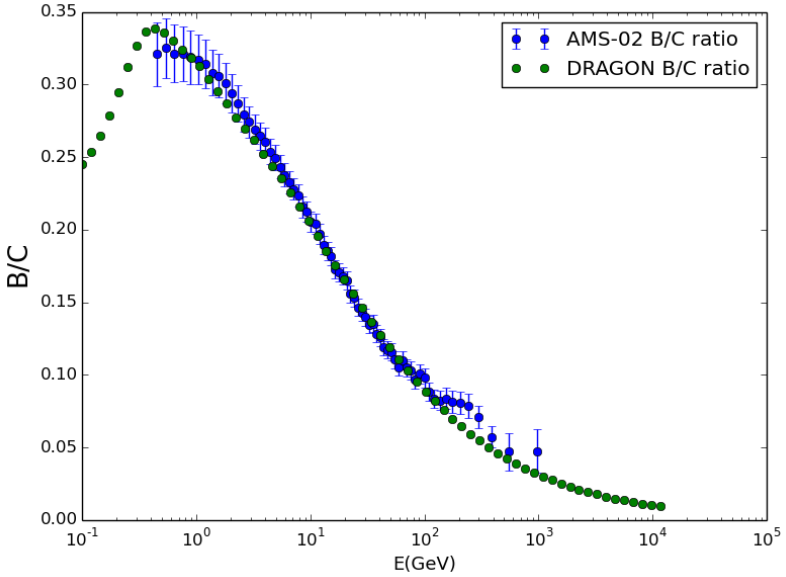

Figure 15: The boron-carbon fit for background with dark matter

4.4 Implications for the propagation parameters

The parameters found that give the best results are presented in appendix B. The difference between the propagation parameters for both fits have some variation when going from an $\bar{p}/p$ fit to the $\bar{p}/p$ with B/C fit. The largest difference for the background scenario is in the v_A parameter, with a total difference of 1066.4%. The smallest variation is at Z_t, where the parameters differ by 6.9%. The average difference is 213.5% for all parameters, 185.5% for the injection spectrum and 246.1% for the propagation parameters.
With the addition of a dark matter signal the difference is reduced with almost one order of magnitude. Both the largest and smallest difference are in the injection spectrum, being ρ_1 and α_1 respectively with 63.4% and 1.7%. The average difference is 16.7%: 16.1% for the injection spectrum, 17.7% for the propagation parameters and 15.3% for $\langle \sigma v \rangle$.
These differences are to be expected when looking at the original B/C spectrum. The addition of dark matter annihilation resulted in a B/C ratio that is much closer to the AMS-02 measurements than the corresponding results with just the background. Therefore only a small correction is needed for the dark matter added case to fit both ratios, while for just the background large differences had to be made to produce an acceptable B/C fit.

5 Conclusion and Outlook

The AMS-02 $\bar{p}/p$ ratio has been analyzed with the DRAGON propagation code to find a possible dark matter signal. The annihilation spectrum was used for a dark matter particle of 85 GeV and the dark matter mass distribution has been set to an NFW profile with a local density of 41 GeV/cm^3. The DRAGON parameters influence the diffusion coefficient, injection spectrum and the size of the galactic halo. For a scenario of dark matter an additional parameter was used, namely the velocity weighted cross-section to define the amount of dark-matter produced particles.
The obtained results show promising prospects for the analysis of dark matter signals in cosmic ray propagation. With the most important finding being that particles originating from dark matter annihilation produce a significant impact on the $\bar{p}/p$ ratio when using the spectrum presented in section 2.1. While the results from the fits cannot be interpreted in a way that either confirms or excludes this dark matter model, bearing in mind that the globally best fit might not yet have been obtained, the quality of the fits of the ratios are satisfactory with the exception of the background model for $\bar{p}/p$ and B/C. With an updated search algorithm the global minima should be able to be found, enabling valid interpretations of the found data.
That however does not mean that these results can be trusted without scepticism. Keeping in mind the uncertainties on the structure of the Milky way and the approximations made by DRAGON, a spectrum provided by DRAGON will never be fully accurate. The combined fit of $\bar{p}/p$ with B/C does constrain the parameters to be physically correct, but caution has to be used when fixing parameters for a $\bar{p}/p$ ratio with the B/C spectrum, since B/C has a different injection spectrum and slight differences in propagation compared to (anti)protons.
Further research has to be done with the first step being a search for the global minima. Furthermore various dark matter models can be used, which could have different annihilation spectra and therefore different effects. Models found by other studies can either be supported or excluded by these searches.
In conclusion, the results from DRAGON will always have some uncertainty, so conservative interpretations have to be used. However, the results are promising and with further research the realm of cosmic ray analysis will provide additional information in the search for dark matter.

References

[1] B. Fuchs, S. Frink, S. Röser, R. Wielen, *Proper motion study of the galactic rotation curve*, Blitz, L., Teuben, P. (eds.): Unsolved problems of the Milky Way. Proc. IAU Symp. 169, Den Haag, The Netherlands, 23-27 August 1994; Kluwer, Dordrecht, p. 689, 1996IAUS..169..689F'

[2] G. Gentile, P. Salucci, U. Klein, D. Vergani and P. Kalberia, *The cored distribution of dark matter in spiral galaxies*, MNRAS 351 (2004) 903

[3] R. Massey, T. Kitching and J. Richard, *The dark matter of gravitational lensing*, Rep. Prog. Phys. 73 (2010) 086901, arXiv:1001.1739 [astro-ph.CO]

[4] M.S. Turner, *Dark Matter and Dark Energy in the universe*, Physica Scripta, Volume 2000, T85

[5] P.J. Fox, R. Harnik, J. Kopp and Y. Tsai, *Missing energy signatures of dark matter at the LHC*, Phys. Rev. D85 (2012) 056011

[6] LUX Collaboration, *First Results from the LUX Dark Matter Experiment at the Sanford Underground Research Facility*, Phys. Rev. Lett. 112 (2014) 091303

[7] A.W. Strong, I.V. Moskalenko and V.S. Ptuskin, *Cosmic-ray propagation and interactions in the Galaxy*, Ann. Rev. Nucl. Part. Sci. 57 (2007) 285, arXiv:astro-ph/0701517

[8] A. Achterberg, S. Amoroso, S. Caron, L. Hendriks, R. Ruiz de Austri and C. Weniger, *A description of the Galactic Center excess in the Minimal Supersymmetric Standard Model*, JCAP 08 (2015) 006, arXiv:1502.05703

[9] A. Achterberg, M. van Beekveld, W. Beenakker, S. Caron and L. Hendriks, *Comparing Galactic Center MSSM dark matter solutions to the Reticulum II gamma-ray data*, JCAP 12 (2015) 013, arXiv:1507.04644

[10] R. Donato, D. maurin, P. Salati, A. Barrau, G. Boudoul and R. Taillet, *Antiprotons from spallations of cosmic rays on interstellar matter*, Astrophys. J. 563 (2001) 172, arXiv:astro-ph/0103150

[11] S.P. Martin, *A Supersymmetry primer*, arXiv:hep-ph/9709356

[12] J.L. Feng, *Supersymmetry and cosmology*, arXiv:hep-ph/0405215

[13] J. Würzinger, *A Dark Matter Simulation of the Galactic Centre Photon Excess in the pMSSM and an Estimation of the Uncertainties*, BSc. thesis (Radboud University, 2016)

[14] AMS collaboration, *The first five years of AMS on the International Space Station*, `http://uhnatsci.org/files/news/AMSPressRelease.pdf`

[15] AMS-02 collaboration, *First Result from the Alpha Magnetic Spectrometer on the International Space Station: Precision Measurement of the Positron Fraction in Primary Cosmic Rays of 0.5-350 GeV*, Phys. Rev. Lett. 110, (2013) 141102

[16] AMS collaboration, *The Alpha Magnetic Spectrometer on the International Space Station*, Int. J. Mod. Phys. E21 (2012) 1230005

[17] I.A. Grenier, J.H. Black, A.W. Strong, *The Nine Lives of Cosmic Rays in Galaxies*, Annu. Rev. Astron. Astrophys. 53 (2015) 199

[18] J.A. Simpson, *Elemental and isotopic composition of the galactic cosmic rays*, Ann. Rev. Nucl. Part. Sci. 33 (1983) 323

[19] S. Hayakawa, K. Ito and Y. Terashima, *Origin of Cosmic Rays*, Prog. Theor. Phys. Supplement 6 (1958) 1-92.

[20] C. Evoli, I. Cholis, D. Grasso, L. Maccione and P. Ullio, *Antiprotons from dark matter annihilation in the Galaxy: astrophysical uncertainties*, Phys. Rev. D85 (2012) 123511, arXiv:1108.0664.

[21] V.S. Berezinskii, S.V. Bulanov, V.A Dogiel, V.L. Ginzburg V.S. Ptuskin, *The astrophysics of cosmic rays*, Amsterdam: North-Holland, 1990

[22] R. Beck, *Magnetic fields in the Milky Way and other spiral galaxies*, Ap&SS 289 (2004) 293, arXiv:astro-ph/0310287

[23] M. Haverkorn, *Magnetic fields in the Milky way*, arXiv:1406.0283

[24] J.C. Brown, 2010, Astronomical Society of the Pacific Conference Series, 438, 216

[25] E.G. Zweibel and C. Heiles, *Magnetic fields in galaxies and beyond*, Nature 385 (1997) 131

[26] J. Han, *New knowledge of the Galactic magnetic fields*, Nucl Phys. Proc. Suppl. 175 (2008) 62, arXiv:0901.0040 [astro-ph.GA]

[27] E.C. Stone, A.C. Cummings, F.B. McDonald, B.C. Heikkila, N. Lal, W.R. Webber, *Voyager 1 observes low-energy galactic cosmic rays in a region depleted of heliospheric ions.*, Science 341 (2013) 150

[28] K.M. Ferriere, *The Interstellar Environment of our Galaxy*, Rev. Mod. Phys. 73 (2001) 1031, arXiv:astro-ph/0106359

[29] V. Formato, on behalf of the AMS-02 collaboration, *Precision Measurement of Boron-to-Carbon ratio in Cosmic Rays from 2 GV to 2 TV with the Alpha Magnetic Spectrometer on the International Space Station*, arXiv:1612.09160 [astro-ph.HE]

[30] L. Maccione, D. Gaggero, C. Evoli, D. Grasso, *DRAGON: Galactic Cosmic Ray Diffusion Code*, Astrophysics Source Code Library, record ascl:1106.011

[31] D. Gaggero, *Cosmic Ray diffusion in the Galaxy and diffuse Gamma emission*, `https://etd.adm.unipi.it/theses/available/etd-10092011-000248/unrestricted/PhD_thesis_Daniele_Gaggero_2011_FINAL.pdf`

[32] C.M. Oishi, J.Y. Yuan, J.A. Cuminato and D.E. Stewart, *Stability analysis of Crank-Nicolson and Euler schemes for time-dependent diffusion equations*, Bit Numer Math 55 (2015) 487

Appendix

Appendix A

Due to the high energies of the particles dealt with, relativistic mechanics are needed to accurately describe the synchrotron motion of cosmic rays in the galactic magnetic fields. Starting with the basic equations $\vec{F} = \frac{d\vec{p}}{dt}$ and $\vec{F} = q(\vec{E} + \vec{v} \times \vec{B})$. In special relativity the momentum reads $\vec{p} = \gamma(v)m\vec{v}$. Because γ is velocity dependent it has to be taken into account when formally deriving the relativistic force. In this case however it is not needed because the magnetic field only provides a perpendicular force. So $v = |\vec{v}|$ does not change, and $\vec{F} = \gamma m \frac{d\vec{v}}{dt}$. It should be noted that technically $|\vec{v}|$ does change due to energy losses in the form of synchrotron radiation, this is however a small change, so it can be ignored.
Now take a homogeneous magnetic field pointing along the z-axis, such that $\vec{B} = B\hat{z}$, and a particle that has velocity $\vec{v} = v_x\hat{x} + v_y\hat{y} + v_z\hat{z}$. The equations of motion become

$$\gamma m \left(\frac{dv_x}{dt}\hat{x} + \frac{dv_y}{dt}\hat{y} + \frac{dv_z}{dt}\hat{z} \right) = q(v_x\hat{x} + v_y\hat{y} + v_z\hat{z}) \times B\hat{z} = qv_yB\hat{x} - qv_xB\hat{y} \Rightarrow \gamma m\ddot{y} = -q\dot{x}B \quad (12)$$

$$\gamma m\ddot{x} = q\dot{y}B \quad (13)$$

$$\gamma m\ddot{z} = 0 \quad (14)$$

Differentiating equation (13) and substituting it in equation (12) the following expression arises: $\dddot{x} = -\left(\frac{qB}{\gamma m}\right)^2 \dot{x}$. When integrating with respect to time the following expression is the result: $\ddot{x} = -\left(\frac{qB}{\gamma m}\right)^2 x + C \equiv -\left(\frac{qB}{\gamma m}\right)^2 (x - x_0)$. The remaining expression is the equation of motion for the harmonic oscillator with an angular frequency of $\omega = \frac{qB}{\gamma m}$ and equilibrium position x_0 and similarly y_0. Using $vsin(\theta) = \omega r \Rightarrow r = \frac{vsin(\theta)}{\omega}$ the synchrotron radius perpendicular to the z-axis can be found. The term $sin(\theta)$ indicates the angle between the velocity and the B-field. For the velocity the following expression can be used

$$E = \gamma mc^2 \quad (15)$$

$$\gamma = \frac{E}{mc^2} \quad (16)$$

$$1 - \left(\frac{v}{c}\right)^2 = \left(\frac{mc^2}{E}\right)^2 \quad (17)$$

$$v = c\sqrt{1 - \left(\frac{mc^2}{E}\right)^2} \quad (18)$$

Putting all of this together we get

$$r = \frac{c\sqrt{1 - \left(\frac{mc^2}{E}\right)^2}}{\left(\frac{qB}{\gamma m}\right)} sin(\theta) = \frac{\gamma mc\sqrt{1 - \left(\frac{mc^2}{E}\right)^2}}{qB} sin(\theta) \quad (19)$$

Appendix B

Table 1: The DRAGON parameters for a fit to the $\bar{p}/p$ ratio.

Parameters	Background	Background with DM
L	7.73805899498	5.21312903397
D_0	2.41515413117	3.37343713811
δ	0.586825696293	0.598732904457
η_T	0.570375135241	0.947740598722
v_A	18.8346198216	3.71737078266
Z_t	35.5683652287	13.0068111513
α_0	1.23891464102	0.992283821085
ρ_0	1.48734580455	3.35614089902
α_1	1.86906363966	2.27189248302
ρ_1	28.939207173	28.939207173
α_2	2.44199212361	2.27564491641
ρ_2	386.769089539	278.932276555
α_3	1.9262806044	1.71695749049
$\langle\sigma v\rangle$		1.53866556536

Table 2: The DRAGON parameters for a fit to the $\bar{p}/p$ and B/C ratios.

Parameters	Background	Background with DM
L	6.00209078374	4.63292445071
D_0	5.01965620059	4.02102779312
δ	0.478807046365	0.508326540108
η_T	0.189547309857	0.828294889098
v_A	0.170543631572	2.87786446451
Z_t	38.203720012	11.2199052718
α_0	0.117098458916	0.856224945782
ρ_0	2.55324540673	3.18760686866
α_1	2.23283891951	2.2360555204
ρ_1	11.1183785201	17.6929624191
α_2	2.26808091844	2.32251765734
ρ_2	743.987559348	245.845020451
α_3	1.5753136526	1.92363446788
$\langle\sigma v\rangle$		1.82279083051

All the parameters are given in standard DRAGON units.

Appendix C

```
<?xml version="3.0.2" ?>
<Output>
  <partialstore /> <!-- The code writes the spectrum at Sun position for each
      species on a FITS file (optional) -->
  <fullstore />    <!-- The code writes the complete (r,z,p) grid of propagated
      particles for each species on a FITS file (optional) -->
  <feedback value="1" />
</Output>
<Grid type="2D">          <!-- Number of spatial dimensions. Options: 2D, 3D -->
  <Observer>
    <x value="8.3" />
    <y value="0.0" />
    <z value="0.0" />
  </Observer>
  <Rmax value="12" />   <!-- Maximum value of Galactocentric radius (R) in kpc -->
  <L value="Variable" />       <!-- Halo size in kpc. The Galaxy extends from -L to
      L -->
  <DimR value="41" />   <!-- Number of grid points along R -->
  <DimZ value="81" />   <!-- Number of grid points along vertical axis -->
  <Ekmin value=".1" />       <!-- Miminum kinetic energy of propagated particles in
      GeV -->
  <Ekmax value="10000." />   <!-- Maximum kinetic energy of propagated particles in
      GeV -->
  <Ekfactor value="1.2" /> <!-- Logaritmic spacing of energy grid. E[i] = exp( ln(
      Ekmin) + i ln(Ekfactor) ) -->
  <NuclearChain>
    <Zmax value="14" />    <!-- Maximum atomic number of propagated particles -->
    <Zmin value="1" />     <!-- Minimum atomic number of propagated particles -->
    <PropLepton />         <!-- The code propagates leptonic species (optional) -->
    <PropExtraComponent />
    <PropSecAntiProton />
  </NuclearChain>
</Grid>
<Algorithm>
  <OpSplit>
    <!-- The code starts with dt = Dtmax; after Nrept iterations, the code rescales
        dt by the factor Dtfactor; this process is iterated until Dtmin is reached
        -->
    <Nrept value="30" />          <!-- Number of iterations before changing timestep
        -->
    <Dtfactor value=".25" />      <!-- Rescaling factor of the time step     -->
    <Dtmin value="0.001" />       <!-- Minimum time step in Myr -->
    <Dtmax value="64." />         <!-- Maximum time step in Myr -->
  </OpSplit>
</Algorithm>
<Galaxy>
  <Gas type="Galprop" />   <!-- Gas model; options: BronfFerr, NS, Galprop, Uniform
      -->
  <SNR type="Ferriere" /> <!-- Source distribution for the primary components;
      options: Lorimer, Galprop, Ferriere, OneRing, Rings -->
  <SNR_Extra type="Ferriere" /> <!-- Source distribution for the extra component;
      options: the same as SNRType (optional) -->
  <XCOmode type="SM96" />        <!-- Model for the X_CO factor; options: SM96,
      galprop_2004, galprop_2010, constant -->
  <Diffusion type="Constant"> <!-- Spatial distribution of the diffusion coefficient
      ; options: Constant, Exp, Qtau -->
```

```
43      <D0_1e28 value="Variable" />   <!-- Normalization of the diffusion coefficient
            at reference rigidity DiffRefRig Unit: 10^28 cm^2/s -->
44      <DiffRefRig value = "4" /> <!-- Reference rigidity for the normalization of the
            diffusion coefficient -->
45      <Delta value="Variable" <!-- Slope of the diffusion coefficient spectrum -->
46      <zt value="Variable"          <!-- Scale heigth of the diffusion coefficient,
            useful in Exp mode: D(z) \propto exp(z/zt) (optional) -->
47      <etaT value="Variable" />       <!-- Low energy correction factor of the
            diffusion coefficient: D \propto beta^etaT  -->
48    </Diffusion>
49    <Reacceleration type="Ptuskin94"> <!-- Optional block -->
50      <vA_kms value="Variable" />          <!-- Alfv n velocity in km/s -->
51    </Reacceleration>
52    <CrossSection type="GalpropXSec" leptopt="Kamae" apopt="GalpropFunction" ApCs="2"
          /> <!-- Model for cross sections. leptopt is the model for electron and
          positron production; options: Kamae, GalpropTable -->
53    <MagneticField type="Pshirkov"> <!-- Model for the magnetic field. Options:
          Pshirkov, Farrar, Uniform, Toymodel -->
54       <B0disk value="2.e-06" /> <!-- Useful for Pshirkov field: halo regular field
             normalization in Gauss -->
55       <B0halo value="4.e-06" /> <!-- Useful for Pshirkov field: turbulent regular
             field normalization in Gauss -->
56       <B0turb value="7.5e-06" />
57    </MagneticField>
58  </Galaxy>
59
60  <CR>
61    <ProtNormEn_GeV value="10" /> <!-- Reference energy for nuclei normalization in
          GeV -->
62    <ElNormEn_GeV value="33." />   <!-- Reference energy for primary electron
          normalization in GeV -->
63    <AntiProtNormEn_GeV value="10" />
64    <AntiProtNormFlux value="4.67e-3" />
65    <ProtNormFlux value="2.72e1" /> <!-- Proton flux at reference energy   for
          normalization; in DRAGON units: GeV^-1 m^-2 s^-1 sr^-1 -->
66    <ElNormFlux value="0.004" />   <!-- Electron flux at reference energy for
          normalization; in DRAGON units: GeV^-1 m^-2 s^-1 sr^-1 -->
67    <ElNormEnExtra_GeV value="300" />     <!-- Reference energy for primary electron
          extra component normalization in GeV -->
68    <ElNormFluxExtra value="1.e-06" /> <!-- Extra component flux at reference energy;
           in DRAGON units: GeV^-1 m^-2 s^-1 sr^-1 -->
69
70    <!-- ************************* -->
71    <InjectionIndexAllNuclei> <!-- You can add an arbitrary number of breaks!! -->
72      <alpha_0 value="Variable" /> <!-- First injection slope for nuclei -->
73      <rho_0 value="Variable" />     <!-- Position of first break (rigidity) in GV -->
74      <alpha_1 value="Variable" /> <!-- Second injection slope for nuclei -->
75      <rho_1 value="Variable" />    <!-- Position of second break (rigidity) in GV -->
76      <alpha_2 value="Variable" />
77      <rho_2 value="Variable" />
78      <alpha_3 value="Variable" />
79    </InjectionIndexAllNuclei>
80    <!-- ************************* -->
81    <InjectionIndexElectrons> <!-- You can add an arbitrary number of breaks!! -->
82       <rho_0 value="1." />   <!-- Position of first break (rigidity) in GV -->
83       <rho_1 value="5." />
84       <rho_2 value="10." />
85       <alpha_0 value="1.80" /> <!-- First injection slope for electrons -->
```

```
86        <alpha_1 value="1.80" />
87        <alpha_2 value="2.50" />
88        <alpha_3 value="2.50" />
89        <CutoffRigEl value="20000." />
90    </InjectionIndexElectrons>
91    <!-- ************************* -->
92    <InjectionIndexExtraComponent>
93          <rho_0 value="1." />
94          <alpha_0 value="1.85" />
95          <alpha_1 value="1.85" />
96          <CutoffRigExtra value="10000." />
97    </InjectionIndexExtraComponent>
98    <!-- ************************* -->
99  </CR>
100
101 <!-- *************** -->
102 <!-- DARK MATTER PART -->
103 <!-- *************** -->
104 <DarkMatter Reaction="Annihilation" Model="SelfTable" Profile="NFW">
105     <!-- Reaction can be "Annihilation" or "Decay", (spectrum) Model can be "
            SelfTable" or "Delta", (density) Profile can be "Iso", "NFW", "Kra", "Moore"
            , "Einasto" -->
106     <PropDMLepton />        <!-- If this flag is specified, leptons originating from
            DM annihilation/decay are computed -->
107     <PropDMAntiProton />    <!-- If this flag is specified, antiprotons originating
            from DM annihilation/decay are computed -->
108     <Mass value="85." />  <!-- DM particle mass in GeV -->
109 <!-- *************** -->
110     <!-- LifeTime value="1e26" -->    <!-- if Decay is specified, the lifetime in
            seconds -->
111     <SigmaV value="Variable" />          <!-- if Annihilation is specified, the <
            sigma v> in cm^3/2 -->
112 <!-- *************** -->
113     <SSDensity value="0.41" />        <!-- Dark Matter local energy density in GeV/cm
            ^3 -->
114     <EkDelta value="10." />          <!-- if Delta is specified as a spectrum model,
            this is the energy in GeV at which particles are injected -->
115     <LeptonDatafile      value="DM/mumu_1000gev_pos.txt" />
116     <!-- if SelfTable is specified as a spectrum model, this is the datafile with
            the inj spectrum in GeV^-1 for leptons      -->
117     <AntiprotonDatafile value="DM/mumu_1000gev_ap.txt" />
118     <!-- if SelfTable is specified as a spectrum model, this is the datafile with
            the inj spectrum in GeV^-1 for antiprotons -->
119     <!--Channel value="17" /-->
120 </DarkMatter>
121 <!-- *************** -->
122 <!-- *************** -->
```